

Stream and Query-guided Feature Aggregation for Efficient and Effective 3D Occupancy Prediction

Seokha Moon^{1,3,†}, Janghyun Baek¹, Giseop Kim^{2,3,‡}, Jinkyu Kim¹, Sunwook Choi³

¹Korea University ²DGIST ³NAVER LABS

<https://github.com/moonseokha/DuOcc>

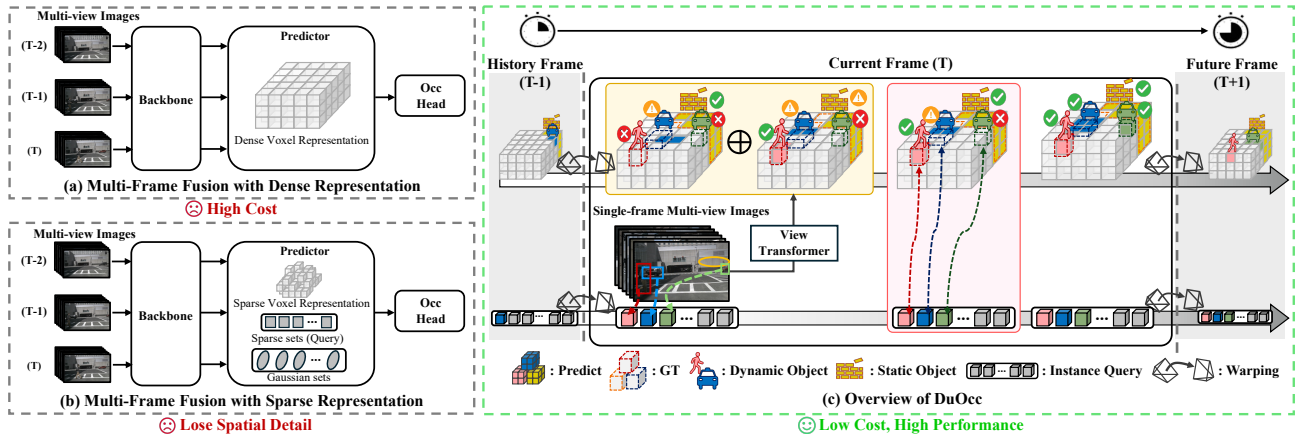


Figure 1. Existing multi-frame fusion based methods leverage temporal information by processing multiple frames. (a) Methods using dense representations [32, 42] preserve spatiotemporal detail but incur high computational cost, and (b) methods based on sparse representations [8, 13, 14, 30, 40] are more efficient yet inevitably lose spatial information. In contrast, (c) our proposed DuOcc maintains dense voxel representations through stream-based and query-guided aggregation, achieving low cost and high spatial fidelity.

Abstract

3D occupancy prediction has become a key perception task in autonomous driving, as it enables comprehensive scene understanding. Recent methods enhance this understanding by incorporating spatiotemporal information through multi-frame fusion, but they suffer from a trade-off: dense voxel-based representations provide high accuracy at significant computational cost, whereas sparse representations improve efficiency but lose spatial detail. To mitigate this trade-off, we introduce *DuOcc*, which employs a dual aggregation strategy that retains dense voxel representations to preserve spatial fidelity while maintaining high efficiency. *DuOcc* consists of two key components: (i) *Stream-based Voxel Aggregation*, which recurrently accumulates voxel features over time and refines them to suppress warping-induced distortions, preserving a clear separation between occupied and free space. (ii) *Query-guided Aggregation*, which complements the limitations of voxel accumulation by selectively injecting instance-level query

features into the voxel regions occupied by dynamic objects. Experiments on the widely used *Occ3D-nuScenes* and *SurroundOcc* datasets demonstrate that *DuOcc* achieves state-of-the-art performance in real-time settings, while reducing memory usage by over 40% compared to prior methods.

1. Introduction

Vision-based 3D occupancy prediction has become a key perception task for autonomous vehicles, enabling safe navigation in dense urban environments. However, relying on a single-frame input severely limits observability and provides insufficient 3D spatial cues, making it difficult to understand the surrounding environment [21, 43]. To address this, recent works [10, 23, 24, 32, 38, 42] leverage temporal context through multi-frame fusion while maintaining dense voxel representations, as shown in Fig. 1(a). This approach effectively integrates spatiotemporal information without sacrificing spatial detail. However, densely processing multiple frames requires substantial computational resources, typically consuming 5–12 GB of GPU memory

[†]Work done during an internship at NAVER LABS.

[‡]Work done at NAVER LABS.

and inducing high inference latency (213–1,250 ms), making these methods impractical for deployment on vehicles.

Towards efficient 3D occupancy prediction, some methods replace dense voxel representations with z-axis pooled BEV features [8, 9], or adopt sparse voxel [30], sparse query sets [40], or Gaussians [13, 14, 51], as illustrated in Fig. 1(b). Although these approaches improve computational efficiency, their dependence on feature compression or sparse encodings inevitably leads to spatial information loss, making it challenging to preserve fine-grained geometry and object boundaries. Furthermore, they still rely on multi-frame processing and require a large number of sparse elements (e.g., queries or Gaussians) to achieve sufficiently dense prediction coverage. Consequently, these methods continue to face an accuracy–efficiency trade-off, limiting their practicality for autonomous driving systems that require low latency, low memory usage, and high accuracy.

To mitigate this trade-off, we extend the recurrent fusion paradigm (i.e., the stream-based approach) to 3D occupancy prediction. Stream-based perception has proven effective for leveraging temporal information in various tasks [4, 6, 28, 37, 41, 46]. However, existing stream-based methods [28, 37, 41] that utilize sparse representations are effective for sparse prediction tasks such as detecting static objects (e.g., sidewalk, drive surface) or dynamic objects (e.g., car, pedestrian), but are unsuitable for dense prediction because they struggle to capture fine-grained spatial detail. These limitations motivate us to extend the recurrent paradigm while maintaining dense representations for 3D occupancy prediction, which requires voxel-level classification of static objects, dynamic objects, and free space. This requirement makes the task more complex and introduces two key challenges when adopting a stream-based paradigm with dense representations: (i) mitigating warping-induced distortions to clearly separate occupied and free space while preserving object boundaries, and (ii) handling dynamic objects, whose voxel representations often lose detail during image-to-voxel projection or become misaligned due to motion.

Our proposed method, DuOcc, addresses these challenges with a dual aggregation strategy designed to effectively handle both static and dynamic object features. As shown in Fig. 1(c), we first warp the voxel features from the immediate previous timestep (which contain accumulated information), apply lightweight refinement to suppress warping-induced distortions and to emphasize object-occupied regions, and then fuse the refined features with voxel features from the current input. While stream-based accumulation effectively handles static structures with consistent spatial alignment, it struggles to capture dynamic objects, making their temporal aggregation unreliable. This difficulty arises from several issues: motion-induced spatial misalignment, sparse projection when distant objects

occupy fewer pixels in the image, collapsed instance boundaries in coarse voxel grids, and loss of semantic cues due to occlusion. Accordingly, we introduce the Query-guided Aggregation module, which leverages instance queries, including those that are temporally propagated and encode fine-grained dynamic object features obtained from image space. These queries are selectively injected into the corresponding voxel regions to recover occluded or missing features (see Fig. 5), thereby complementing stream-based accumulation for dynamic object representation.

We demonstrate that DuOcc matches or surpasses the performance of state-of-the-art methods on the widely used Occ3D-nuScenes [39] and SurroundOcc [43] datasets, achieving +2.3/+1.1 mIoU (in a real-time setting), while maintaining low computational cost. In particular, DuOcc requires only 2.8GB of GPU memory and runs at 83.3 ms.

2. Related Work

2.1. 3D Occupancy Prediction

3D occupancy prediction is a dense prediction task that reconstructs the surrounding environment in voxel space for holistic 3D understanding. Early methods adopted dense representations such as BEV features, which lift 2D semantics into a 3D voxel space [11, 20, 23], while later approaches [24, 39, 43, 48] further enhanced voxel quality through multi-scale encoding and depth–semantic fusion. However, using only a single frame limits visibility in occluded regions and results in sparse feature projection, leading to incomplete reconstructions. To address this, multi-frame fusion approaches [10, 24, 32, 38, 42] jointly process consecutive frames to improve temporal consistency, achieving strong performance. Yet, their dense voxel fusion across frames incurs substantial computational cost, including high memory usage and latency. In pursuit of higher efficiency, recent methods adopt sparse or compressed representations: TPVFormer [12] compresses voxels into tri-plane features, while SparseOcc [30], FastOcc [9], and OPUS [40] focus computation on occupied regions. More recently, Gaussian-based methods [13, 14, 35, 51] have emerged as efficiency-oriented alternatives. However, these approaches still face a trade-off between geometric precision and computational efficiency: sparse Gaussians lose significant spatial detail, whereas dense Gaussians preserve more detail but require higher computational cost. Overall, achieving a balance between spatial fidelity and efficiency remains the central challenge in 3D occupancy prediction.

2.2. Stream-based 3D Perception

To reduce the cost of processing multiple frames, stream-based approaches recurrently update features over time and have shown strong performance across diverse perception tasks [3, 4, 6, 17–19, 25, 27–29, 37, 41, 45–47]. However,

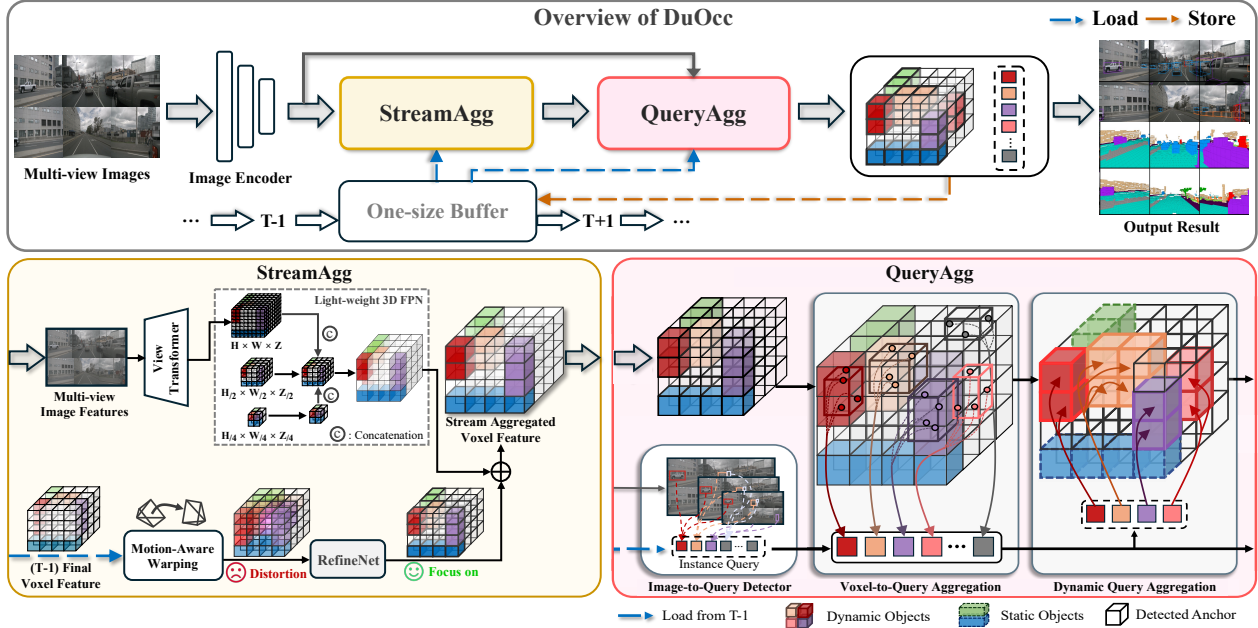


Figure 2. Overview of *DuOcc*, which predicts the 3D occupancy state of each voxel in a streaming manner with dual aggregation strategy. First, voxel features are recurrently accumulated over time through Stream-based Voxel Feature Aggregation (StreamAgg), which efficiently handles features of stationary objects. These temporally aggregated features are then further refined using Query-guided Aggregation (QueryAgg), which utilizes instance queries that encode fine-grained, instance-level features to enhance the representation of non-stationary (dynamic) objects.

methods using sparse representations [4, 18, 27, 28, 37, 41, 47] are mainly suited for object-level tasks such as detecting dynamic agents or static map elements, and their sparsity inherently loses fine structural details, limiting applicability to the dense voxel reasoning required for 3D occupancy prediction. GaussianWorld [51] extends the sparse stream-based paradigm to 3D occupancy prediction using temporal Gaussian updates, but reconstructing complete geometry still demands numerous Gaussians, increasing computational cost. In contrast, stream-based methods that utilize dense representations [3, 6, 17, 19, 25, 29, 45, 46] recurrently update dense BEV features, effectively preserving spatiotemporal context and reducing information loss, making them more suitable for dense prediction tasks. Motivated by this, we extend the dense streaming paradigm to the 3D occupancy prediction task, which requires voxel-level classification of both static and dynamic objects as well as free space, making it more complex. Such complexity raises new challenges, and to address them, we propose *DuOcc*, which employs a dual aggregation strategy to effectively apply the stream-based paradigm while maintaining dense voxel representations.

3. Method

We present a 3D occupancy prediction model that processes multi-view images using a dual aggregation strategy. As illustrated in Fig.2, the framework consists of two main modules: StreamAgg (Sec.3.1), which recurrently ac-

cumulates voxel features to preserve spatiotemporal context and mitigate warping-induced distortions through a lightweight refinement module, RefineNet; and QueryAgg (Sec. 3.2), which compensates for dynamic object features that voxel accumulation alone struggles to capture by injecting instance-level information from sequentially updated instance queries.

3.1. Stream-based Voxel Feature Aggregation

In this section, we describe the four key components of Stream-based Voxel Feature Aggregation (StreamAgg): (i) how voxel features are extracted from multi-view images, (ii) how temporal information is aggregated across frames, (iii) how warping distortions are mitigated, and (iv) how the refinement process is guided by auxiliary supervision.

2D-to-3D View Transformation. Given a set of N multi-view images at timestep t , $\{I_i^t\}$ for $i \in \{1, 2, \dots, N\}$, we extract multi-scale 2D features F_i using a ResNet [7] with FPN [26], following prior works [8, 10, 32]. These features are then projected into a unified 3D voxel space via a 2D-to-3D view transformation [21], producing an initial voxel feature $\mathbf{V}_{\text{init}}^t \in \mathbb{R}^{C_{\text{init}} \times X \times Y \times Z}$, where X , Y , and Z denote the voxel grid dimensions. We then apply a lightweight 3D-FPN to aggregate multi-level voxel features and obtain the current downsampled voxel feature $\mathbf{V}_{\text{curr}}^t \in \mathbb{R}^{C \times \frac{X}{2} \times \frac{Y}{2} \times \frac{Z}{2}}$.

Motion-aware Voxel Feature Warping. To integrate temporal information across frames, we align the propagated voxel feature from the previous timestep $\mathbf{V}_{\text{fin}}^{t-1} \in$

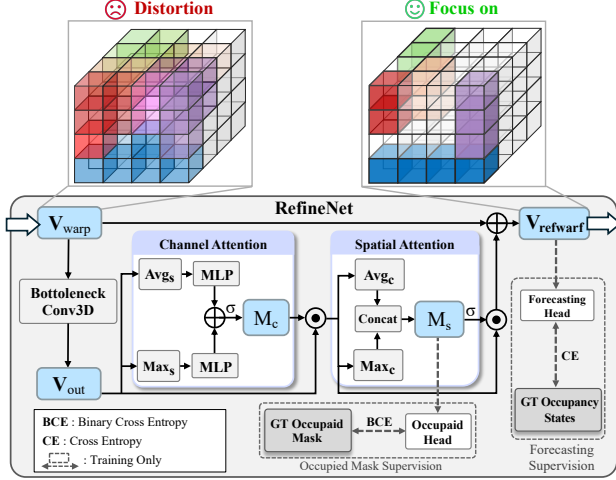


Figure 3. **Overview of the RefineNet** We propose RefineNet to mitigate warping-induced distortions and emphasize object-occupied regions in voxel space. It refines warped features using BottleneckConv3D with 3D channel and spatial attention, selectively enhancing meaningful voxels while suppressing noise. To ensure reliable learning, two auxiliary supervision heads, occupied mask and forecasting, are used only at training time.

$\mathbb{R}^{C \times \frac{X}{2} \times \frac{Y}{2} \times \frac{Z}{2}}$ to the current frame via motion-aware warping. Without such alignment, naive aggregation leads to spatial inconsistencies, degrading the quality of temporally accumulated features in a stream-based manner. Inspired by [10], we transform the spatial coordinates of the previous voxel grid $\mathbf{P}^e(t-1)$ into the current ego-centric coordinate as:

$$\bar{\mathbf{P}}^e(t) = \mathcal{T}_{g \rightarrow e}^t \cdot \mathcal{T}_{e \rightarrow g}^{t-1} \cdot \mathbf{P}^e(t-1), \quad (1)$$

where $\mathcal{T}_{e \rightarrow g}^{t-1}$ maps coordinates from the past ego frame to the global frame, and $\mathcal{T}_{g \rightarrow e}^t$ brings them to the current ego-centric frame. We compute the warped voxel feature as:

$$\mathbf{V}_{\text{warp}}^t(\mathbf{P}^e(t)) = \text{Interp}(\mathbf{V}_{\text{fin}}^{t-1}, \bar{\mathbf{P}}^e(t)), \quad (2)$$

where $\text{Interp}(\cdot)$ denotes trilinear interpolation that maps past features to the current frame while preserving spatial consistency.

Voxel Feature Refinement. The warping process propagates contextual cues from past observations, but it inevitably introduces distortions due to the interpolation mechanism, particularly in empty regions, at object boundaries, and in crowded areas. These distortions can lead to erroneous values or blurred object contours, degrading feature quality and temporal consistency. To mitigate these distortions and preserve consistent spatial detail over time, we introduce RefineNet (see Fig. 3), a lightweight refinement module. RefineNet follows a bottleneck structure [7], which compresses $\mathbf{V}_{\text{warp}}^t \in \mathbb{R}^{C \times \frac{X}{2} \times \frac{Y}{2} \times \frac{Z}{2}}$ to $C/4$ channels, refines and reconstructs them to C channels to produce $\mathbf{V}_{\text{out}}^t$, which reduces computation overhead while maintaining representational capacity. To further encourage Re-

fineNet to selectively enhance meaningful voxel regions, we extend CBAM [44] into 3D space, where channel attention and spatial attention are sequentially applied as follows:

$$\begin{aligned} \mathbf{M}_c &= \sigma(\text{MLP}(\text{Avg}_s(\mathbf{V}_{\text{out}}^t)) + \text{MLP}(\text{Max}_s(\mathbf{V}_{\text{out}}^t))) \\ \mathbf{M}_s &= \text{Conv3D}([\text{Avg}_c(\mathbf{M}_c \odot \mathbf{V}_{\text{out}}^t); \text{Max}_c(\mathbf{M}_c \odot \mathbf{V}_{\text{out}}^t)]), \end{aligned} \quad (3)$$

where σ denotes the sigmoid function, Avg_s , Max_s denote spatial pooling, and Avg_c , Max_c denote channel pooling. The refined warped feature is computed as:

$$\mathbf{V}_{\text{refwarp}}^t = \sigma(\mathbf{M}_s) \odot (\mathbf{M}_c \odot \mathbf{V}_{\text{out}}^t) + \mathbf{V}_{\text{warp}}^t, \quad (4)$$

Finally, the refined warped feature is fused with the current voxel feature to obtain the Stream Aggregated voxel feature:

$$\mathbf{V}_{\text{S.A}}^t = \mathbf{V}_{\text{refwarp}}^t + \mathbf{V}_{\text{curr}}^t. \quad (5)$$

Supervision for RefineNet. To ensure that RefineNet reliably learns to adjust voxel features, we incorporate two auxiliary supervision heads used only at training time. *Occupied Mask supervision*, we upsample the spatial attention feature \mathbf{M}_s to the original voxel resolution and apply the MLP-based decoder as the Occupied Head (following the same architecture described in Sec. 3.3) to predict a binary occupancy map $\mathbf{V}_{\text{bin}}^t \in \mathbb{R}^{1 \times X \times Y \times Z}$. The prediction is supervised with the ground-truth occupied mask via binary cross-entropy loss, encouraging the refinement module to emphasize occupied voxels while suppressing empty or noisy regions. *Forecasting Supervision*, following the idea of temporally consistent feature supervision [16, 33], the refined warped voxel feature is further used to predict the voxel occupancy state at the current timestep using the same upsampling and MLP-based decoder architecture, as the Forecasting Head.

3.2. Query-guided Aggregation

To complement the representation of dynamic objects that are difficult to capture through voxel feature accumulation alone, we propose Query-guided Aggregation (QueryAgg). QueryAgg recurrently updates instance queries that encode dynamic object semantics from multi-level image features, and aggregates these query features into the corresponding voxel regions occupied by those objects. As shown in Fig. 2, this module consists of three components: Image-to-Query Detector, Voxel-to-Query Aggregation, and Dynamic Query Aggregation.

Image-to-Query Detector (I2Q). Since dynamic object representations are difficult to capture when relying solely on voxel feature accumulation, we extract richer object-specific information directly from image space. To this end, we adopt an Image-to-Query Detector based on Sparse4Dv3 [28], which aggregates dynamic object semantics from multi-view multi-level image features F_i and en-

codes them into instance queries. These queries are initialized with anchor boxes, then refined via cross-attention with multi-scale image features to incorporate high-resolution visual cues. To integrate temporal information, the queries interact with propagated instance queries from the previous timestep, enabling effective fusion of motion-aware semantics. Finally, each instance query retrieves fine-grained details from regions in F_i at predicted object locations, ensuring precise and robust dynamic object representation.

Voxel-to-Query Aggregation (V2Q). Instance queries obtained from the Image-to-Query Detector offer rich semantics and approximate localization, but suffer from depth ambiguity due to the limitations of monocular perception. Conversely, voxel representations provide reliable 3D geometric information but lack fine-grained semantic cues for dynamic objects. Leveraging the complementary characteristics of these two representations, we introduce Voxel-to-Query Aggregation to mitigate the depth uncertainty inherent in instance queries by incorporating 3D geometric information from $\mathbf{V}_{S.A.}^t$. Specifically, we refine each query feature using deformable attention [49] to selectively sample informative regions in the voxel space. The query feature q_{vox}^i is updated as:

$$q_{\text{vox}}^i = q_{\text{img}}^i + \sum_{h=1}^H W_h \left[\sum_{o=1}^O \alpha_{iho} \cdot W_h' \cdot \mathbf{V}_{S.A.}^t(x_i + \Delta x_{iho}, y_i + \Delta y_{iho}, z_i + \Delta z_{iho}) \right], \quad (6)$$

where q_{img}^i is the instance feature from the Image-to-Query Detector, and (x_i, y_i, z_i) is the query’s center. H and O denote the number of attention heads and sampling points, respectively. Each head refines sampling positions using offsets $(\Delta x_{iho}, \Delta y_{iho}, \Delta z_{iho})$, weighted by attention scores α_{iho} . Learnable matrices W_h and W_h' transform query and voxel features. This process guides queries to informative 3D regions, enhancing spatial and depth representations.

Dynamic Query Aggregation (DQA). To selectively aggregate instance-level features from successfully detected dynamic objects into corresponding voxel grid cells, we introduce Dynamic Query Aggregation (DQA). DQA first filters high-confidence instance queries based on a predefined threshold (see the supplementary material). The selected queries are then mapped to the voxel grids occupied by the corresponding object, and query-to-voxel attention aggregates their features as follows:

$$\begin{aligned} \mathbf{q}^i &= \mathbf{W}_Q (\mathbf{V}_{S.A.}^i + \sigma_p), \quad \mathbf{k}^{ij} = \mathbf{v}^{ij} = \mathbf{W}_{K/V} q_{\text{vox}}^{ij}, \quad (7) \\ \alpha^i &= \text{softmax} \left(\frac{\mathbf{q}^{i\top}}{\sqrt{d}} \cdot [\mathbf{k}^{ij}]_{j \in \mathcal{N}^i} \right), \quad \mathbf{z}^i = \sum_{j \in \mathcal{N}^i} \alpha^{ij} \cdot \mathbf{v}^{ij}, \quad (8) \\ \mathbf{g}^i &= \text{sigmoid} (\mathbf{W}^{\text{gate}} [\mathbf{V}_{S.A.}^i, \mathbf{z}^i]). \quad (9) \end{aligned}$$

Here, \mathcal{N}^i denotes the set of instance queries whose bound-

ing boxes overlap with the i -th voxel grid cell, allowing DQA to selectively update only those voxels likely containing dynamic objects while ignoring static or empty regions to reduce computational cost. The query, key, and value features are denoted by \mathbf{q}^i , \mathbf{k}^{ij} , and \mathbf{v}^{ij} , respectively, obtained via linear projections \mathbf{W}_Q , \mathbf{W}_K , and \mathbf{W}_V . To encode spatial context, \mathbf{q}^i is formed by adding positional encoding σ_p to the reference voxel feature $\mathbf{V}_{S.A.}^i$. Attention weights α^{ij} measure the relevance between voxel i and instance query j , producing the aggregated feature \mathbf{z}^i . A gating mechanism parameterized by \mathbf{W}^{gate} then modulates \mathbf{z}^i before integrating it with $\mathbf{V}_{S.A.}^i$, enabling the voxel representation to adaptively aggregate instance-level information.

For voxels without overlapping queries ($\mathcal{N}^i = \emptyset$), the features remain unchanged:

$$\mathbf{V}_{\text{DQA}}^i = \begin{cases} \mathbf{V}_{S.A.}^i, & \text{if } \mathcal{N}^i = \emptyset, \\ \mathbf{V}_{S.A.}^i + \mathbf{g}^i \odot \mathbf{z}^i, & \text{otherwise.} \end{cases} \quad (10)$$

The updated voxel features \mathbf{V}_{DQA} are passed through a feed-forward network with normalization and residual connections, producing the final voxel feature \mathbf{V}_{fin} , which is fed into the occupancy head for 3D occupancy prediction.

3.3. Decoder for Occupancy Prediction

To predict the high-resolution 3D voxel occupancy, we upsample the final voxel feature \mathbf{V}_{fin} to obtain $\mathbf{V}_{\text{up}} \in \mathbb{R}^{C \times X \times Y \times Z}$, which is then processed by a lightweight MLP-based decoder used in both training and inference. To further enhance semantic representation learning without modifying the voxel features, we incorporate an Auxiliary Mask Decoder inspired by Co-DETR [50], adopting the multi-head transformer-based mask prediction design from the Semantic-aware Group Decoder in COTR [32]. During training, a group-wise one-to-many assignment associates each ground-truth mask with multiple queries, providing richer supervision. As this auxiliary decoder is used solely for feature learning, it is omitted at inference time to avoid unnecessary computation and maintain efficiency.

4. Experiments

4.1. Datasets

We evaluate our method on two benchmark datasets for 3D occupancy prediction: Occ3D-nuScenes [39] and SurroundOcc dataset [43]. Both datasets represent the scene as a voxel grid of size $200 \times 200 \times 16$, where each voxel is labeled as either *occupied* or *empty*, and occupied voxels are further categorized into 16 semantic classes such as *car* and *pedestrian*. **Occ3D-nuScenes** defines the voxel grid in the ego coordinate, spanning $[-40\text{m}, 40\text{m}]$ along both X and Y and $[-1\text{m}, 5.4\text{m}]$ along Z , discretized at a resolution of 0.4m, with occupied voxels assigned to 17

semantic classes (16 known categories + others). **SurroundOcc dataset**, in contrast, defines the voxel grid in the LiDAR coordinate, covering $[-50\text{m}, 50\text{m}]$ along X and Y and $[-5\text{m}, 3\text{m}]$ along Z , with a voxel resolution of 0.5m.

4.2. Implementation and Evaluation Details

Following standard practice [8, 10, 15, 32, 38], we adopt ResNet-50 [7] as the image backbone and resize all input images to 256×704 . The initial voxel feature \mathbf{V}_{init} is obtained via the BEVDepth-style view transformer [21], producing a $200 \times 200 \times 16$ voxel grid with 64 channels. For processing dynamic objects, we use 900 instance queries, and the auxiliary mask decoder consists of 6 heads. The model is trained using AdamW [31] for 24 epochs on Occ3D-nuScenes and 20 epochs on SurroundOcc, with a batch size of 8, gradient clipping, an initial learning rate of 2×10^{-4} , and a warmup ratio of 1/3 over the first 200 iterations. Inference speed and GPU memory usage are measured on an NVIDIA A100 GPU and an RTX 4090 GPU.

Further, following common practice [2, 39, 43], we evaluate occupancy prediction using mean IoU (mIoU) over semantic classes, and additionally report class-agnostic IoU to assess overall 3D geometry reconstruction by treating all occupied voxels as foreground. The Image-to-Query detector used in QueryAgg is evaluated using nuScenes Detection Score (NDS) [1] and mean Average Precision (mAP).

4.3. Comparison with SOTA Methods

We evaluate DuOcc on the Occ3D-nuScenes [39] dataset (Tab. 1). Even with only StreamAgg, DuOcc* already outperforms existing real-time methods, achieving 40.4 mIoU with the shortest latency and lowest memory usage. With the full dual aggregation strategy, DuOcc reaches 41.9 mIoU while still operating in real time (83.3 ms), surpassing approaches that rely on multi-frame fusion combined with sparse representations, such as FastOcc [9], OPUS [40], and GSD-Occ [8]. Moreover, DuOcc outperforms non-real-time dense voxel aggregation methods: it runs over 4× faster than PanoOcc [42], and although COTR [32] attains the highest accuracy, DuOcc is 13× faster while using more than 4× less memory than both models. These results highlight the accuracy–efficiency balance of DuOcc.

On the SurroundOcc [43] dataset (Tab. 2), DuOcc likewise achieves the best overall performance, improving both IoU and mIoU over Gaussian-based methods [13, 14], and even outperforming GaussianWorld [51], which also applies a stream-based approach with Gaussians. Notably, DuOcc is the only method that satisfies the real-time constraint while using over 40% less memory than all competing approaches.

We further evaluate methods using RayIoU [30] (Tab. 3), which measures the consistency of occupancy prediction along viewing rays. DuOcc achieves the highest overall

Table 1. We report performance on the Occ3D-nuScenes dataset [39] in terms of mIoU, inference latency (Lat., measured in ms on one NVIDIA A100 GPU), and memory consumption (Mem., measured in MB). Methods with latency in the near real-time ($\approx 100\text{ms}$) are highlighted in gray. Among these, best and second-best results are shown in **bold** and underlined, respectively. (* denotes our method performing with only StreamAgg)

Method	Backbone	Input Type	mIoU \uparrow	Lat.	Mem.
SurroundOcc [43]	ResNet-101	900×1600	37.1	312.5	5,491
FB-OCC [24]	ResNet-50	256×704	37.5	142.8	5,467
BEVFormer [23]	ResNet-101	900×1600	39.3	212.7	6,651
BEVDet4D [10]	ResNet-50	256×704	39.2	1,250.0	6,053
PanoOcc [42]	ResNet-101	864×1600	41.6	333.3	11,991
COTR [32]	ResNet-50	256×704	44.5	1,111.1	10,453
FastOcc [9]	ResNet-101	320×800	37.2	90.3	-
SparseOcc [30]	ResNet-50	256×704	30.9	56.5	6,883
OPUS [40]	ResNet-50	256×704	35.6	75.7	6,735
ProtoOcc [34]	ResNet-50	256×704	37.8	105.0	-
GSD-Occ [8]	ResNet-50	256×704	39.4	<u>50.0</u>	4,759
ProtoOcc [15]	ResNet-50	256×704	39.6	77.9	-
DuOcc*	ResNet-50	256×704	<u>40.4</u>	49.0	2,437
DuOcc (Ours)	ResNet-50	256×704	41.9	83.3	2,788

Table 2. We report performance on the SurroundOcc dataset [43] in terms of IoU, mIoU, inference latency (Lat., measured in ms on one NVIDIA 4090 GPU), and memory consumption (Mem., measured in MB). Among these, best results are shown in **bold**.

Method	IoU \uparrow	mIoU \uparrow	Lat. (ms)	Mem. (MB)
BEVFormer [23]	30.5	16.8	241	6,651
TPVFormer [12]	30.9	17.1	320	5,100
SurroundOcc [43]	31.5	20.3	344	5,491
GaussianFormer [13]	29.8	19.1	372	6,229
GaussianFormer-2 [14]	30.4	19.7	451	4,535
GaussianWorld [51]	33.0	21.9	228	7,030
DuOcc (ours)	33.4	23.0	84	2,788

Table 3. 3D occupancy prediction performance evaluated using RayIoU, as proposed by [30]. Results are reported on the Occ3D-nuScenes dataset [39] without using the visibility mask for training, under a real-time inference setting (≤ 100 ms).

Method	RayIoU	RayIoU _{1m}	RayIoU _{2m}	RayIoU _{4m}
SparseOcc [30]	35.1	29.1	35.8	40.3
GSD-Occ [8]	38.9	33.0	39.7	44.1
ODG [35]	39.2	-	-	-
OPUS [40]	40.3	33.7	41.1	46.0
DuOcc (Ours)	41.1	34.2	41.9	47.1

RayIoU (41.1), consistently outperforming prior real-time approaches. Together, these results demonstrate that DuOcc provides state-of-the-art accuracy while maintaining practical runtime and memory efficiency, making it practical for real-world deployment.

Qualitative results in Fig. 4 also demonstrate that DuOcc more precisely reconstructs the surrounding environment compared to the previous state-of-the-art real-time method GSD-Occ [8], yielding clearer representations of dynamic objects (Rows 1–2) and static structures (Row 3).

Table 4. Ablation study on the Occ3D-nuScenes dataset. Evaluates the effect of each component of DuOcc in terms of overall mIoU (mIoU_A), dynamic and static object mIoU (mIoU_D and mIoU_S, respectively), and per-class performance.

Method	mIoU ↑			mIoU ↑ (Dynamic Objects)										mIoU ↑ (Static Objects)					
	mIoU _A ↑	mIoU _D ↑	mIoU _S ↑	barrier	bicycle	bus	car	cons. veh.	motorcycle	pedestrian	traffic cone	trailer	truck	drive. surf.	other flat	sidewalk	terrain	manmade	vegetation
GSD-Occ [8]	39.4	35.1	51.2	46.2	27.8	46.0	50.5	27.1	27.7	29.0	28.1	31.2	37.8	80.9	42.5	50.5	54.8	41.3	36.9
A. Base	36.8	32.6	48.5	44.1	22.4	44.9	50.0	21.2	23.9	25.7	25.4	32.0	36.3	78.9	41.0	48.5	51.4	38.1	32.9
B. A + StreamAgg	40.4	35.4	53.4	47.2	26.2	45.5	53.8	24.8	29.4	26.9	29.5	32.8	38.4	83.2	45.6	54.0	57.6	42.7	37.5
C. B + Detection Head	40.8	36.3	53.1	48.0	26.8	46.0	54.6	24.9	29.6	28.6	30.7	33.2	40.9	83.2	45.4	53.8	57.3	41.8	37.4
D. B + QueryAgg (Ours)	41.9	38.1	<u>53.3</u>	50.8	29.6	48.5	56.1	<u>25.4</u>	31.4	30.0	33.0	34.6	41.9	83.3	45.9	<u>53.8</u>	<u>57.3</u>	<u>42.3</u>	<u>37.2</u>

Table 5. Ablation study on StreamAgg.

Method	mIoU ↑	Lat. (ms)	Mem. (MB)
Motion-aware Warping	38.72	43.9	2,423
(+) RefineNet	39.84	49.0	2,437
(+) Supervision (Forecasting)	40.25	49.0	2,437
(+) Supervision (Occupied)	40.37	49.0	2,437

4.4. Effect of DuOcc Components

Tab. 4 presents an ablation study on Occ3D-nuScenes [39]. Base model (A), using only a single-frame, achieves 36.8 mIoU. Adding StreamAgg (B), which sequentially accumulates voxel features over time while preserving spatiotemporal context, boosts performance to 40.4 mIoU. However, (B) still shows a large performance gap between static and dynamic objects (53.4 vs. 35.4), indicating voxel accumulation struggles with dynamic objects. Model (C) adds a detection head for dynamic object supervision, achieving limited gain (+0.9 mIoU on dynamic objects) due to the lack of direct feature-level injection. In contrast, model (D) integrates QueryAgg, which directly injects dynamic object features into the corresponding voxel regions. This targeted aggregation improves performance on dynamic objects by +2.7 mIoU compared to (B) and increases overall mIoU to 41.90, while maintaining performance on static objects. Moreover, DuOcc surpasses the previous real-time state-of-the-art GSD-Occ [8] across most object classes, demonstrating the effectiveness of our framework.

4.5. Effect of StreamAgg Components

Tab. 5 shows the effect of each component in StreamAgg. Motion-aware Warping provides the fundamental improvement by aligning voxel features across frames, while adding RefineNet further mitigates warping artifacts, boosting performance to 39.84 mIoU. Forecasting supervision improves temporal consistency, and Occupied Mask supervision encourages the refinement to focus on object-occupied voxels, resulting in the best performance (40.37 mIoU) without additional computational cost. Overall, each component con-

Table 6. Ablation study on QueryAgg.

Model	Component			Metrics		
	I2Q	V2Q	DQA	mIoU ↑	NDS ↑	mAP ↑
A				40.37	–	–
B		✓		40.06	0.4704	0.3458
C	✓			40.42	0.4904	0.3516
D	✓	✓		40.78	0.4964	0.3620
E	✓	✓	✓	41.90	0.5001	0.3681

Table 7. Ablation study on image-to-voxel aggregation. S.A: StreamAgg, SCA: Spatial Cross-Attention, Q.A: QueryAgg.

Model	mIoU _A	mIoU _D	mIoU _S	Lat. (ms)	Mem. (MB)
S.A only	40.37	35.36	53.42	49.0	2,437
S.A + SCA	40.72	35.77	53.59	95.2	3,554
S.A + Q.A	41.90	38.12	53.31	83.3	2,788

tributes complementary gains, with the full StreamAgg providing a stable and spatially coherent voxel representation.

4.6. How to Utilize a Detector for Joint Learning?

Tab. 6 presents an ablation study on how detectors enhance both detection and occupancy prediction performance. Model (A) is a baseline using only StreamAgg. Model (B) applies a query-based detector on voxel features for multi-task learning, as in [36, 42], but is inefficient due to the large search space and fails to detect objects absent from voxel features. Model (C) employs an Image-to-Query Detector for finer image-based detection but lacks voxel-level supervision, yielding limited gains. Model (D) improves this by combining semantic cues from images with geometric details from voxel features to guide dynamic object localization, yet still lacks direct voxel interaction. Our proposed model (E), DuOcc, directly aggregates instance-level features into voxel features, complementing instance-level feature of dynamic objects. This interactive design enhances both detection and occupancy prediction, which are built upon distinct representations, achieving the highest NDS, mAP, and mIoU.

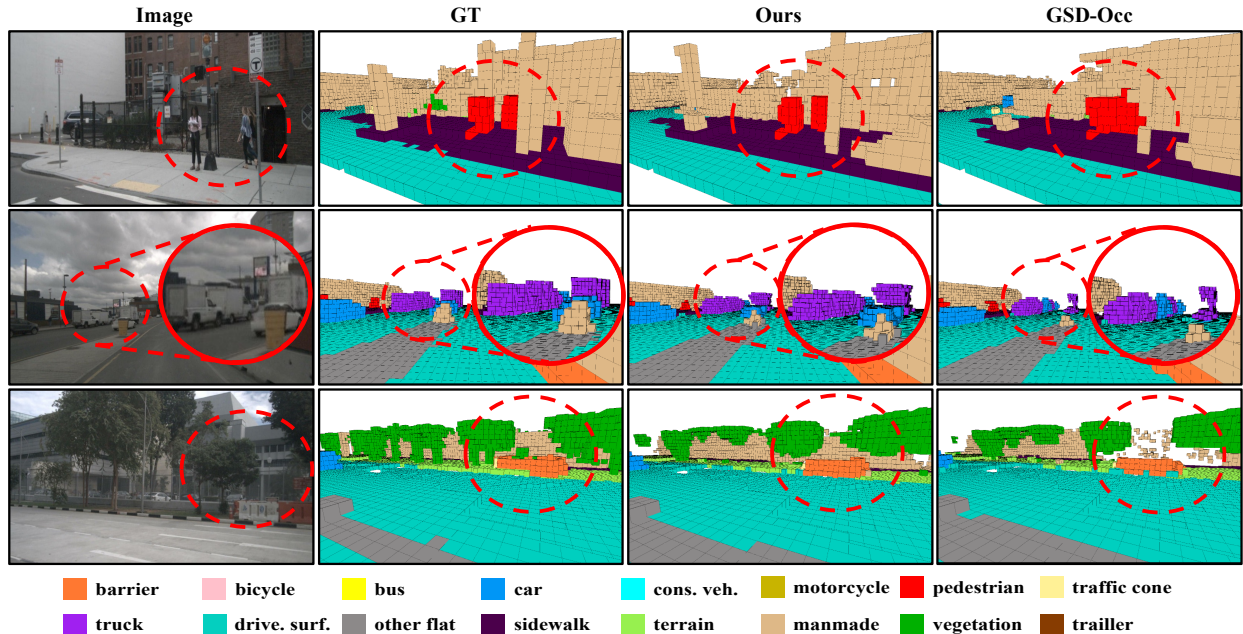


Figure 4. Examples of 3D occupancy prediction results from our proposed method (DuOcc) and GSD-Occ. The corresponding input image and ground-truth 3D occupancy are also provided. Our method demonstrates notably improved prediction quality for both dynamic objects (1st and 2nd rows) and static objects (3rd row). Refer to the dotted circles for a detailed comparison of prediction outputs. More examples are provided in the supplemental material.

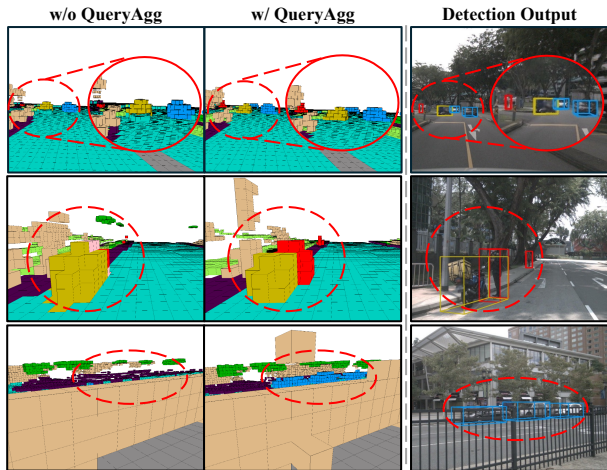


Figure 5. Effect of the QueryAgg, particularly for dynamic objects that are distant, overlapped or occluded. The third column visualizes detection outputs from instance queries used in QueryAgg.

4.7. Effect of Query-guided Aggregation

Tab. 7 compares image-to-voxel aggregation methods for overcoming the limitations of voxel-based encoding. Prior works adopt Spatial Cross-Attention (SCA) [32, 38, 48] to distribute image features across all voxel grids, providing slight improvements. However, spatial misalignment between voxel and image space often leads to hallucinated mappings [22], and the lack of explicit supervision on what to extract and where to place it results in suboptimal performance. In contrast, Query-guided Aggregation (QueryAgg)

explicitly extracts dynamic object features and selectively integrates them into the voxel regions they occupy. This targeted aggregation strategy mitigates hallucinations, reduces unnecessary computation, and yields a +2.76 mIoU gain on dynamic objects and +1.53 overall, while maintaining high efficiency with 83.3 ms latency and 2,788 MB memory.

Fig. 5 shows that QueryAgg effectively enhances the voxel representation of dynamic objects that appear small due to distance, are occluded, or are overlapped by nearby objects. As shown in the detection outputs, instance queries accurately capture each object, thus allowing their fine-grained features to be directly aggregated into the corresponding voxel regions. This explicit instance-level aggregation enables the model to overcome voxel grid limitations and better represent complex scenes.

5. Conclusion

In this paper, we present DuOcc, a 3D occupancy prediction framework with a dual aggregation strategy that balances efficiency and accuracy. By integrating Stream-based Voxel Aggregation and Query-guided Aggregation, it effectively accumulates spatiotemporal information, mitigates warping distortions, and enhances dynamic object representations. DuOcc achieves state-of-the-art performance on the Occ3D-nuScenes and SurroundOcc datasets, reducing memory usage by over 40% under real-time constraints, and jointly predict 3D occupancy and object poses makes it well-suited for downstream tasks in autonomous driving.

References

- [1] Holger Caesar, Varun Bankiti, Alex H Lang, Sourabh Vora, Venice Erin Liong, Qiang Xu, Anush Krishnan, Yu Pan, Giancarlo Baldan, and Oscar Beijbom. nuscenes: A multimodal dataset for autonomous driving. In *CVPR*, pages 11621–11631, 2020. 6
- [2] Anh-Quan Cao and Raoul De Charette. Monoscene: Monocular 3d semantic scene completion. In *Proceedings of the IEEE/CVF Conference on Computer Vision and Pattern Recognition*, pages 3991–4001, 2022. 6
- [3] Ming Chang, Xishan Zhang, Rui Zhang, Zhipeng Zhao, Guanhua He, and Shaoli Liu. Recurrentbev: A long-term temporal fusion framework for multi-view 3d detection. In *European Conference on Computer Vision*, pages 131–147. Springer, 2024. 2, 3
- [4] Xuechao Chen, Shuangjie Xu, Xiaoyi Zou, Tongyi Cao, Dit-Yan Yeung, and Lu Fang. Svqnet: Sparse voxel-adjacent query network for 4d spatio-temporal lidar semantic segmentation. In *Proceedings of the IEEE/CVF International Conference on Computer Vision*, pages 8569–8578, 2023. 2, 3
- [5] Bowen Cheng, Ishan Misra, Alexander G Schwing, Alexander Kirillov, and Rohit Girdhar. Masked-attention mask transformer for universal image segmentation. In *Proceedings of the IEEE/CVF conference on computer vision and pattern recognition*, pages 1290–1299, 2022. 12
- [6] Chunrui Han, Jinrong Yang, Jianjian Sun, Zheng Ge, Runpei Dong, Hongyu Zhou, Weixin Mao, Yuang Peng, and Xiangyu Zhang. Exploring recurrent long-term temporal fusion for multi-view 3d perception. *IEEE Robotics and Automation Letters*, 9(7):6544–6551, 2024. 2, 3
- [7] Kaiming He, Xiangyu Zhang, Shaoqing Ren, and Jian Sun. Deep residual learning for image recognition. In *Proceedings of the IEEE conference on computer vision and pattern recognition*, pages 770–778, 2016. 3, 4, 6
- [8] Yulin He, Wei Chen, Tianci Xun, and Yusong Tan. Real-time 3d occupancy prediction via geometric-semantic disentanglement. *arXiv preprint arXiv:2407.13155*, 2024. 1, 2, 3, 6, 7, 13
- [9] Jiawei Hou, Xiaoyan Li, Wenhao Guan, Gang Zhang, Di Feng, Yuheng Du, Xiangyang Xue, and Jian Pu. Fastocc: Accelerating 3d occupancy prediction by fusing the 2d bird’s-eye view and perspective view. *ICRA*, 2024. 2, 6
- [10] Junjie Huang and Guan Huang. Bevdet4d: Exploit temporal cues in multi-camera 3d object detection. *arXiv preprint arXiv:2203.17054*, 2022. 1, 2, 3, 4, 6
- [11] Junjie Huang, Guan Huang, Zheng Zhu, Yun Ye, and Dalong Du. Bevdet: High-performance multi-camera 3d object detection in bird-eye-view. *arXiv preprint arXiv:2112.11790*, 2021. 2
- [12] Yuanhui Huang, Wenzhao Zheng, Yunpeng Zhang, Jie Zhou, and Jiwen Lu. Tri-perspective view for vision-based 3d semantic occupancy prediction. In *Proceedings of the IEEE/CVF conference on computer vision and pattern recognition*, pages 9223–9232, 2023. 2, 6
- [13] Yuanhui Huang, Wenzhao Zheng, Yunpeng Zhang, Jie Zhou, and Jiwen Lu. Gaussianformer: Scene as gaussians for vision-based 3d semantic occupancy prediction. In *European Conference on Computer Vision*, pages 376–393. Springer, 2024. 1, 2, 6
- [14] Yuanhui Huang, Amonnut Thammatadatrakoon, Wenzhao Zheng, Yunpeng Zhang, Dalong Du, and Jiwen Lu. Gaussianformer-2: Probabilistic gaussian superposition for efficient 3d occupancy prediction. In *Proceedings of the Computer Vision and Pattern Recognition Conference*, pages 27477–27486, 2025. 1, 2, 6
- [15] Jungho Kim, Changwon Kang, Dongyoung Lee, Sehwan Choi, and Jun Won Choi. Protoocc: Accurate, efficient 3d occupancy prediction using dual branch encoder-prototype query decoder. In *Proceedings of the AAAI Conference on Artificial Intelligence*, pages 4284–4292, 2025. 6
- [16] Sanmin Kim, Youngseok Kim, In-Jae Lee, and Dongsuk Kum. Predict to detect: Prediction-guided 3d object detection using sequential images. In *Proceedings of the IEEE/CVF international conference on computer vision*, pages 18057–18066, 2023. 4
- [17] Junho Koh, Youngwoo Lee, Jungho Kim, Dongyoung Lee, and Jun Won Choi. Onlinebev: Recurrent temporal fusion in bird’s eye view representations for multi-camera 3d perception. *IEEE Transactions on Intelligent Transportation Systems*, 2025. 2, 3
- [18] Changcai Li, Zonghua Gu, Gang Chen, Libo Huang, Wei Zhang, and Huihui Zhou. Real-time stereo-based 3d object detection for streaming perception. *Advances in Neural Information Processing Systems*, 37:115468–115490, 2024. 3
- [19] Xiaotian Li, Baojie Fan, Jiandong Tian, and Huijie Fan. Gafusion: Adaptive fusing lidar and camera with multiple guidance for 3d object detection. In *Proceedings of the IEEE/CVF Conference on Computer Vision and Pattern Recognition*, pages 21209–21218, 2024. 2, 3
- [20] Yin hao Li, Han Bao, Zheng Ge, Jinrong Yang, Jianjian Sun, and Zeming Li. Bevstereo: Enhancing depth estimation in multi-view 3d object detection with temporal stereo. In *AAAI*, pages 1486–1494, 2023. 2
- [21] Yin hao Li, Zheng Ge, Guanyi Yu, Jinrong Yang, Zengran Wang, Yukang Shi, Jianjian Sun, and Zeming Li. Bevdepth: Acquisition of reliable depth for multi-view 3d object detection. In *Proceedings of the AAAI Conference on Artificial Intelligence*, pages 1477–1485, 2023. 1, 3, 6, 12
- [22] Yiming Li, Zhiding Yu, Christopher Choy, Chaowei Xiao, Jose M Alvarez, Sanja Fidler, Chen Feng, and Anima Anandkumar. Voxformer: Sparse voxel transformer for camera-based 3d semantic scene completion. In *Proceedings of the IEEE/CVF conference on computer vision and pattern recognition*, pages 9087–9098, 2023. 8
- [23] Zhiqi Li, Wenhao Wang, Hongyang Li, Enze Xie, Chonghao Sima, Tong Lu, Yu Qiao, and Jifeng Dai. Bevformer: Learning bird’s-eye-view representation from multi-camera images via spatiotemporal transformers. In *ECCV*, pages 1–18, 2022. 1, 2, 6
- [24] Zhiqi Li, Zhiding Yu, David Austin, Mingsheng Fang, Shiyi Lan, Jan Kautz, and Jose M Alvarez. Fb-occ: 3d occupancy prediction based on forward-backward view transformation. *arXiv preprint arXiv:2307.01492*, 2023. 1, 2, 6
- [25] Zhenxin Li, Shiyi Lan, Jose M Alvarez, and Zuxuan Wu. Bevnex: Reviving dense bev frameworks for 3d object de-

- tection. In *Proceedings of the IEEE/CVF conference on computer vision and pattern recognition*, pages 20113–20123, 2024. 2, 3
- [26] Tsung-Yi Lin, Piotr Dollár, Ross Girshick, Kaiming He, Bharath Hariharan, and Serge Belongie. Feature pyramid networks for object detection. In *Proceedings of the IEEE conference on computer vision and pattern recognition*, pages 2117–2125, 2017. 3
- [27] Xuewu Lin, Tianwei Lin, Zixiang Pei, Lichao Huang, and Zhizhong Su. Sparse4d v2: Recurrent temporal fusion with sparse model. *arXiv preprint arXiv:2305.14018*, 2023. 2, 3
- [28] Xuewu Lin, Zixiang Pei, Tianwei Lin, Lichao Huang, and Zhizhong Su. Sparse4d v3: Advancing end-to-end 3d detection and tracking. *arXiv preprint arXiv:2311.11722*, 2023. 2, 3, 4, 12
- [29] Haisong Liu, Yao Teng, Tao Lu, Haiguang Wang, and Limin Wang. Sparsebev: High-performance sparse 3d object detection from multi-camera videos. In *Proceedings of the IEEE/CVF international conference on computer vision*, pages 18580–18590, 2023. 2, 3
- [30] Haisong Liu, Haiguang Wang, Yang Chen, Zetong Yang, Jia Zeng, Li Chen, and Limin Wang. Fully sparse 3d panoptic occupancy prediction. *arXiv preprint arXiv:2312.17118*, 2023. 1, 2, 6
- [31] I Loshchilov. Decoupled weight decay regularization. *arXiv preprint arXiv:1711.05101*, 2017. 6
- [32] Qihang Ma, Xin Tan, Yanyun Qu, Lizhuang Ma, Zhizhong Zhang, and Yuan Xie. Cotr: Compact occupancy transformer for vision-based 3d occupancy prediction. In *Proceedings of the IEEE/CVF Conference on Computer Vision and Pattern Recognition*, pages 19936–19945, 2024. 1, 2, 3, 5, 6, 8
- [33] Seokha Moon, Hongbeen Park, Jaekoo Lee, and Jinkyu Kim. Learning temporal cues by predicting objects move for multi-camera 3d object detection. In *2024 IEEE International Conference on Robotics and Automation (ICRA)*, pages 6607–6613. IEEE, 2024. 4
- [34] Gyeongrok Oh, Sungjune Kim, Heeju Ko, Hyung-gun Chi, Jinkyu Kim, Dongwook Lee, Daehyun Ji, Sungjoon Choi, Sujin Jang, and Sangpil Kim. 3d occupancy prediction with low-resolution queries via prototype-aware view transformation. In *Proceedings of the Computer Vision and Pattern Recognition Conference*, pages 17134–17144, 2025. 6
- [35] Yunxiao Shi, Yinhao Zhu, Shizhong Han, Jisoo Jeong, Amin Ansari, Hong Cai, and Fatih Porikli. Odg: Occupancy prediction using dual gaussians. *arXiv preprint arXiv:2506.09417*, 2025. 2, 6
- [36] Chonghao Sima, Wenwen Tong, Tai Wang, Li Chen, Silei Wu, Hanming Deng, Yi Gu, Lewei Lu, Ping Luo, Dahua Lin, et al. Scene as occupancy. *arXiv preprint arXiv:2306.02851*, 2023. 7
- [37] Wenchao Sun, Xuewu Lin, Yining Shi, Chuang Zhang, Hao-ran Wu, and Sifa Zheng. Sparsedrive: End-to-end autonomous driving via sparse scene representation. In *2025 IEEE International Conference on Robotics and Automation (ICRA)*, pages 8795–8801. IEEE, 2025. 2, 3
- [38] Xin Tan, Wenbin Wu, Zhiwei Zhang, Chaojie Fan, Yong Peng, Zhizhong Zhang, Yuan Xie, and Lizhuang Ma. Geocc: Geometrically enhanced 3d occupancy network with implicit-explicit depth fusion and contextual self-supervision. *arXiv preprint arXiv:2405.10591*, 2024. 1, 2, 6, 8
- [39] Xiaoyu Tian, Tao Jiang, Longfei Yun, Yue Wang, Yilun Wang, and Hang Zhao. Occ3d: A large-scale 3d occupancy prediction benchmark for autonomous driving. *arXiv preprint arXiv:2304.14365*, 2023. 2, 5, 6, 7, 13
- [40] Jiabao Wang, Zhaojiang Liu, Qiang Meng, Liujiang Yan, Ke Wang, Jie Yang, Wei Liu, Qibin Hou, and Mingming Cheng. Opus: occupancy prediction using a sparse set. 2024. 1, 2, 6
- [41] Shihao Wang, Yingfei Liu, Tiancai Wang, Ying Li, and Xiangyu Zhang. Exploring object-centric temporal modeling for efficient multi-view 3d object detection. In *Proceedings of the IEEE/CVF International Conference on Computer Vision*, pages 3621–3631, 2023. 2, 3
- [42] Yuqi Wang, Yuntao Chen, Xingyu Liao, Lue Fan, and Zhaoxiang Zhang. Panoocc: Unified occupancy representation for camera-based 3d panoptic segmentation. In *Proceedings of the IEEE/CVF conference on computer vision and pattern recognition*, pages 17158–17168, 2024. 1, 2, 6, 7, 13
- [43] Yi Wei, Linqing Zhao, Wenzhao Zheng, Zheng Zhu, Jie Zhou, and Jiwen Lu. Surroundocc: Multi-camera 3d occupancy prediction for autonomous driving. In *Proceedings of the IEEE/CVF International Conference on Computer Vision*, pages 21729–21740, 2023. 1, 2, 5, 6
- [44] Sanghyun Woo, Jongchan Park, Joon-Young Lee, and In So Kweon. Cbam: Convolutional block attention module. In *Proceedings of the European conference on computer vision (ECCV)*, pages 3–19, 2018. 4
- [45] Junbo Yin, Jianbing Shen, Runnan Chen, Wei Li, Ruigang Yang, Pascal Frossard, and Wenguan Wang. Is-fusion: Instance-scene collaborative fusion for multimodal 3d object detection. In *Proceedings of the IEEE/CVF conference on computer vision and pattern recognition*, pages 14905–14915, 2024. 2, 3
- [46] Tianyuan Yuan, Yicheng Liu, Yue Wang, Yilun Wang, and Hang Zhao. Streammapnet: Streaming mapping network for vectorized online hd map construction. In *Proceedings of the IEEE/CVF Winter Conference on Applications of Computer Vision*, pages 7356–7365, 2024. 2, 3
- [47] Hao Zhang, Constantine Tarabanis, Neil Jethani, Mark Goldstein, Silas Smith, Larry Chinitz, Rajesh Ranganath, Yindalon Aphinyanaphongs, and Lior Jankelson. Qtmet: Predicting drug-induced qt prolongation with artificial intelligence-enabled electrocardiograms. *Clinical Electrophysiology*, 10 (5):956–966, 2024. 2, 3
- [48] Yunpeng Zhang, Zheng Zhu, and Dalong Du. Occformer: Dual-path transformer for vision-based 3d semantic occupancy prediction. In *Proceedings of the IEEE/CVF International Conference on Computer Vision*, pages 9433–9443, 2023. 2, 8
- [49] Xizhou Zhu, Weijie Su, Lewei Lu, Bin Li, Xiaogang Wang, and Jifeng Dai. Deformable detr: Deformable transformers for end-to-end object detection. *arXiv preprint arXiv:2010.04159*, 2020. 5
- [50] Zhuofan Zong, Guanglu Song, and Yu Liu. Detrs with collaborative hybrid assignments training. In *Proceedings of*

the IEEE/CVF international conference on computer vision, pages 6748–6758, 2023. [5](#), [12](#)

- [51] Sicheng Zuo, Wenzhao Zheng, Yuanhui Huang, Jie Zhou, and Jiwen Lu. Gaussianworld: Gaussian world model for streaming 3d occupancy prediction. In *Proceedings of the Computer Vision and Pattern Recognition Conference*, pages 6772–6781, 2025. [2](#), [3](#), [6](#)

Stream and Query-guided Feature Aggregation for Efficient and Effective 3D Occupancy Prediction

Supplementary Material

A. Further Implementation Details

A.1. Lightweight 3D-FPN

Following BEVDepth [21], we lift image features into the 3D voxel space, obtaining $\mathbf{V}_{\text{init}} \in \mathbb{R}^{C \times X \times Y \times Z}$, which encodes both spatial and semantic information and serves as the foundation for 3D occupancy prediction. To improve computational efficiency while preserving essential structure, we apply a lightweight 3D-FPN that downsamples voxel features, avoiding excessively fine voxel grids that introduce unnecessary computation.

Specifically, \mathbf{V}_{init} is passed through a Conv3D block to generate multi-scale voxel features: $\mathbf{V}_1 \in \mathbb{R}^{C_1 \times \frac{X}{2} \times \frac{Y}{2} \times \frac{Z}{2}}$ and $\mathbf{V}_2 \in \mathbb{R}^{C_2 \times \frac{X}{4} \times \frac{Y}{4} \times \frac{Z}{4}}$. These features, together with \mathbf{V}_{init} , are then uniformly resampled to a resolution of $\frac{X}{2} \times \frac{Y}{2} \times \frac{Z}{2}$ via trilinear interpolation. The interpolated volumes are concatenated and compressed using a Conv1D layer to obtain a compact representation $\mathbf{V}_{\text{curr}} \in \mathbb{R}^{C \times \frac{X}{2} \times \frac{Y}{2} \times \frac{Z}{2}}$. This design substantially reduces computational overhead while maintaining spatial and semantic detail.

A.2. Query Selection for Dynamic Query Aggregation

In Dynamic Query Aggregation (DQA), the query selection process is carefully designed to avoid issues that arise when selecting queries based solely on IoU with ground-truth. This approach risks mapping all queries close to ground-truth into voxel features, regardless of whether those queries are well-detected or not. Consequently, the voxel features are trained with an implicit reliance on ground-truth information, leading to incorrect learning and overfitting.

To overcome this issue, we adopt filtering criteria during training that combine IoU with ground-truth, confidence scores, and geometric constraints to ensure reliable integration of instance-level information while maintaining model generalization. For large objects, queries are selected if they satisfy an IoU threshold of 0.4 and a confidence score above 0.3. For small objects, even slight deviations between ground-truth bounding boxes and predicted bounding boxes can result in poor IoU, making it difficult to capture queries that accurately detect small objects in 3D space. Therefore, we introduce a geometric constraint-based metric that utilizes the center point deviation D_{center} and the box size deviation D_{size} , ensuring that $(\sigma_c \cdot D_{\text{center}} + \sigma_b \cdot D_{\text{size}}) < 1.5$, where σ_c and σ_b are empirically set to 2.0 and 1.0, respectively. This approach compensates for the limitations of IoU and ensures reliable query selection for small objects in 3D

space.

During inference, the filtering process is simplified to select only instance queries with a confidence score above 0.3, consistent with the detection threshold. These strategies allow DQA to integrate reliable instance-level information while enabling the model to generalize effectively while ensuring robust detection of dynamic objects.

A.3. Decoder

At each timestep t , our 3D occupancy decoder outputs the semantic voxel volume $\mathbf{Y}_t \in \{y_0, y_1, \dots, y_C\}^{X \times Y \times Z}$ denotes the number of semantic classes and y_0 corresponds to empty space, with X , Y , and Z representing the voxel volume’s spatial dimensions. From the final voxel feature \mathbf{V}_{fin} , we apply a 3D deconvolution to obtain the upsampled feature $\mathbf{V}_{\text{up}} \in \mathbb{R}^{C \times X \times Y \times Z}$, which is then decoded by a lightweight MLP to produce per-voxel semantics. The same decoding procedure is applied in the RefineNet forecasting head using $\mathbf{V}_{\text{refwarp}}$, as well as in the occupied head, which takes \mathbf{M}_s to determine whether each voxel in the $X \times Y \times Z$ space is occupied or empty. Additionally, to further enhance semantic representation learning, we apply an auxiliary mask decoder built upon \mathbf{V}_{fin} , following Co-DETR [50]; this module adopts multiple Mask2Former-based [5] heads to predict per-class occupancy masks.

A.4. Loss Functions

To optimize our model, we combine multiple task-specific loss functions. For depth estimation, we adopt the depth loss $\mathcal{L}_{\text{depth}}$ from BEVDepth [21]. Voxel occupancy prediction uses the cross-entropy-based occupancy loss \mathcal{L}_{occ} , applied to the predictions generated by an MLP on P_{fin} . The Image-to-Query Detector utilizes the detection loss \mathcal{L}_{det} from Sparse4D v3 [28]. To improve voxel representation, we incorporate an Auxiliary Mask Decoder with the mask loss $\mathcal{L}_{\text{mask}}$, as described in Mask2Former [5].

In addition, the forecasting head refines the warped historical voxel features by predicting the corrected current occupancy distribution, which is supervised using a cross-entropy loss $\mathcal{L}_{\text{fore}}$. The occupied mask head determines whether each voxel is filled or empty and is supervised with a binary cross-entropy loss \mathcal{L}_{bin} . The total loss function $\mathcal{L}_{\text{total}}$ is defined as:

$$\mathcal{L}_{\text{total}} = \lambda_{\text{depth}} \cdot \mathcal{L}_{\text{depth}} + \lambda_{\text{occ}} \cdot \mathcal{L}_{\text{occ}} + \lambda_{\text{det}} \cdot \mathcal{L}_{\text{det}} + \lambda_{\text{mask}} \cdot \mathcal{L}_{\text{mask}} + \lambda_{\text{fore}} \cdot \mathcal{L}_{\text{fore}} + \lambda_{\text{bin}} \cdot \mathcal{L}_{\text{bin}}, \quad (11)$$

where λ_{depth} , λ_{occ} , λ_{det} , λ_{mask} , λ_{fore} , and λ_{bin} are the balancing weights for each loss term. In our experiments, we

empirically set these weights to 0.05, 10.0, 0.2, 1.0, 10.0, and 10.0 respectively.

B. More Experiments

B.1. Comparison of Computational Efficiency

Table 8 reports the computational cost and accuracy comparison on the Occ3D-nuScenes [39] dataset. Compared to existing methods [8, 42], DuOcc achieves the best balance between efficiency and performance. GSD-Occ relies on a parameter-heavy design, while PanoOcc incurs extremely large FLOPs because it processes multi-frame inputs using a dense voxel representation, which significantly increases the computational burden. In contrast, DuOcc architecture attains a highly favorable trade-off by reducing FLOPs and parameters simultaneously while improving accuracy. Specifically, it requires only 418GFLOPs and 49M parameters, representing 35.4% and 57.0% reductions over GSD-Occ, respectively, while improving mIoU by +2.5. Moreover, compared to PanoOcc, which uses fewer parameters but suffers from exceptionally high computational load, DuOcc delivers higher accuracy (41.9 vs. 41.6 mIoU) with only 10.7% of its FLOPs. These results demonstrate that DuOcc achieves state-of-the-art performance with drastically improved computational efficiency, making it well suited for real-time and resource-constrained deployment.

Table 8. Comparison of computational efficiency and performance on the Occ3D-nuScenes dataset [39].

Method	FLOPs(G)↓	Params↓	mIoU↑
GSD-Occ [8]	647	114M	39.4
PanoOcc [42]	3900	56M	41.6
DuOcc (Ours)	418	49M	41.9

B.2. More visualization

Figure 6 further demonstrates the performance of DuOcc across three distinct scenarios, comparing the ground truth, results without QueryAgg, results with QueryAgg, and detection outputs from the instance queries. The first row enhances the representation of distant pedestrians, while the second row illustrates its ability to separate nearby objects and accurately capture their occupancy. The third row demonstrates how DQA enables the occupancy map to capture a truck that is partially obscured by a fence. Since the fence obstructs the truck in the image view, its semantic information is not well projected into the 3D space. However, by leveraging QueryAgg, the model directly aggregates object-level information, allowing the truck to be accurately represented in the occupancy map. Additionally, Figures 7 to 10 visualize the model’s performance in complex scenarios.

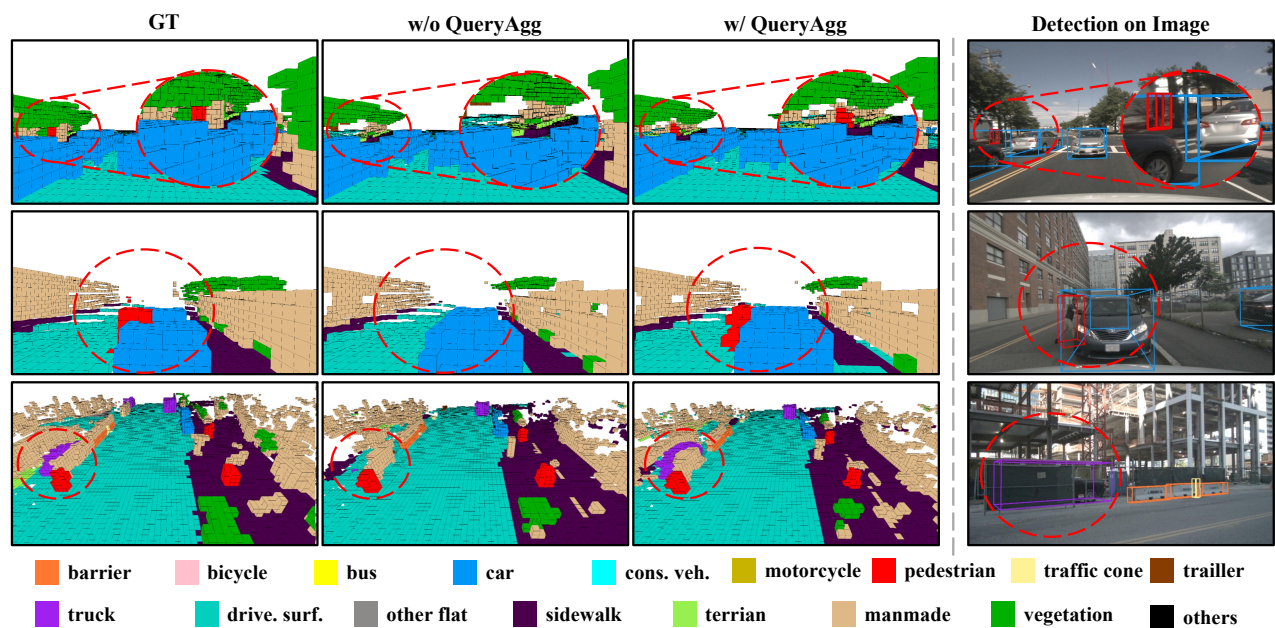


Figure 6. Visualization results of DuOcc across three distinct scenarios. Each row shows the ground-truth (GT), results without QueryAgg (w/o QueryAgg), with QueryAgg (w/ QueryAgg), and detection outputs from the instance queries.

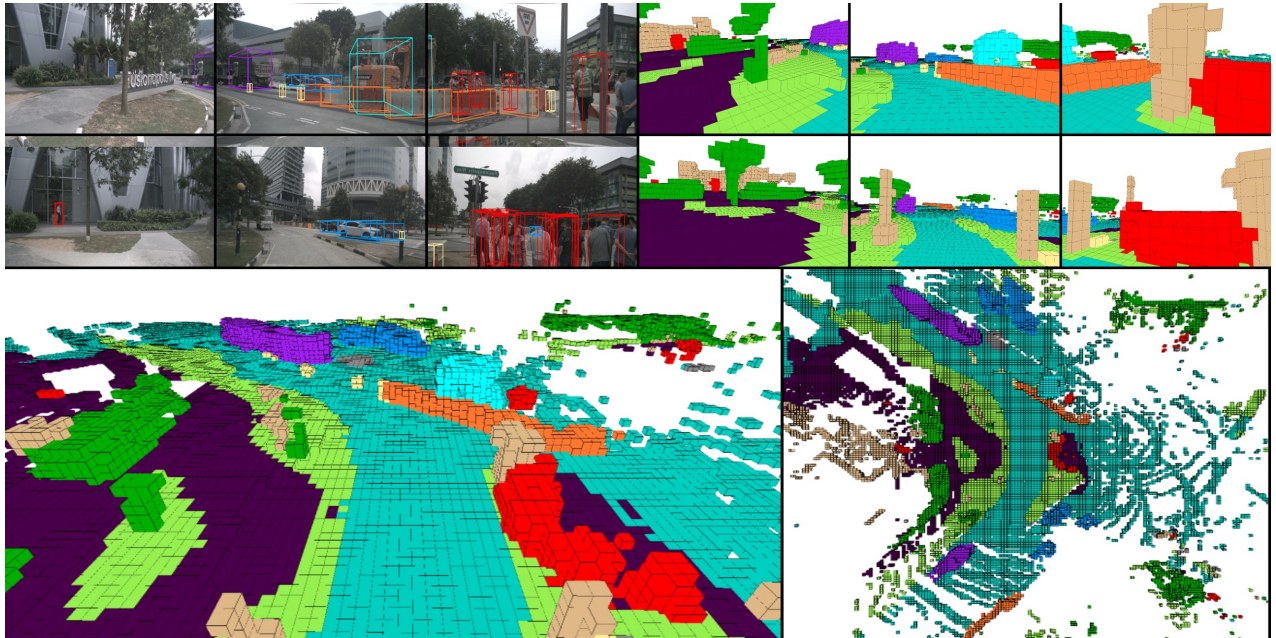


Figure 7. Visualization of 3D occupancy prediction in a dynamic urban scene with construction and pedestrians. The top-left shows object detection on the images, the top-right presents occupancy prediction in the camera view, the bottom-left illustrates the top-front view, and the bottom-right depicts the top-down occupancy prediction results.

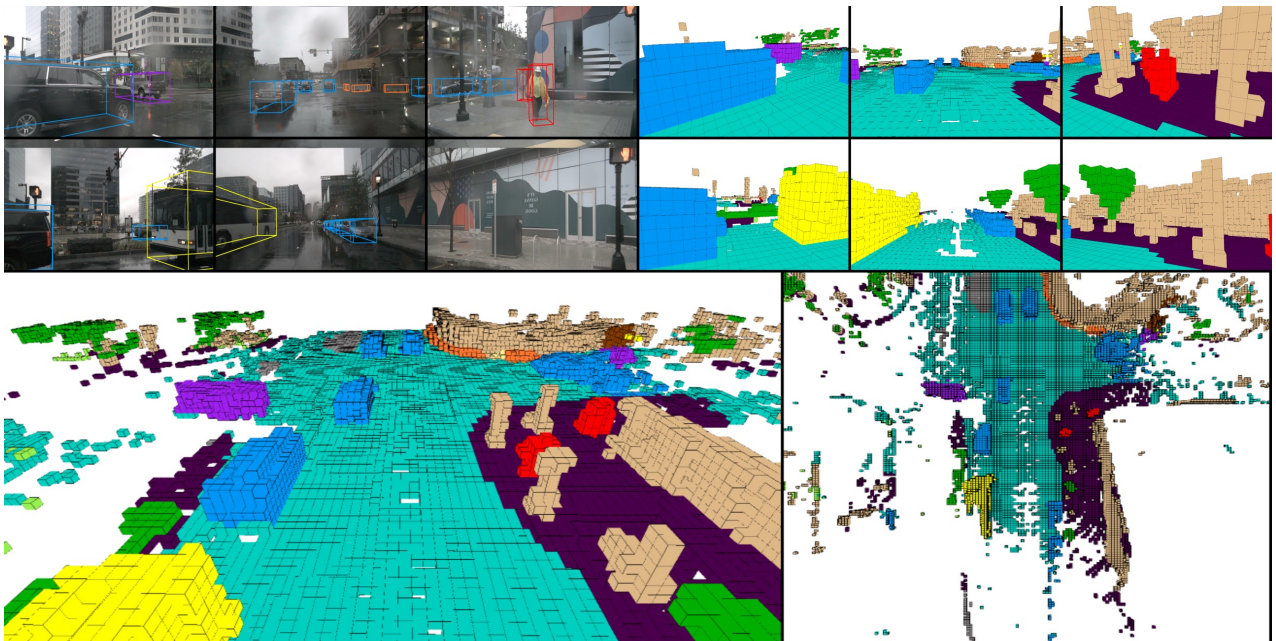


Figure 8. Visualization of 3D occupancy prediction at a crowded intersection on a rainy day. The top-left shows object detection in the image space, the top-right presents occupancy prediction in the camera view, the bottom-left illustrates the top-front view, and the bottom-right depicts the top-down occupancy prediction results.

- | | | | | | | | | |
|---------|--------------|------------|----------|------------|------------|------------|--------------|---------|
| barrier | bicycle | bus | car | cons. veh. | motorcycle | pedestrian | traffic cone | trailer |
| truck | drive. surf. | other flat | sidewalk | terrain | manmade | vegetation | others | |

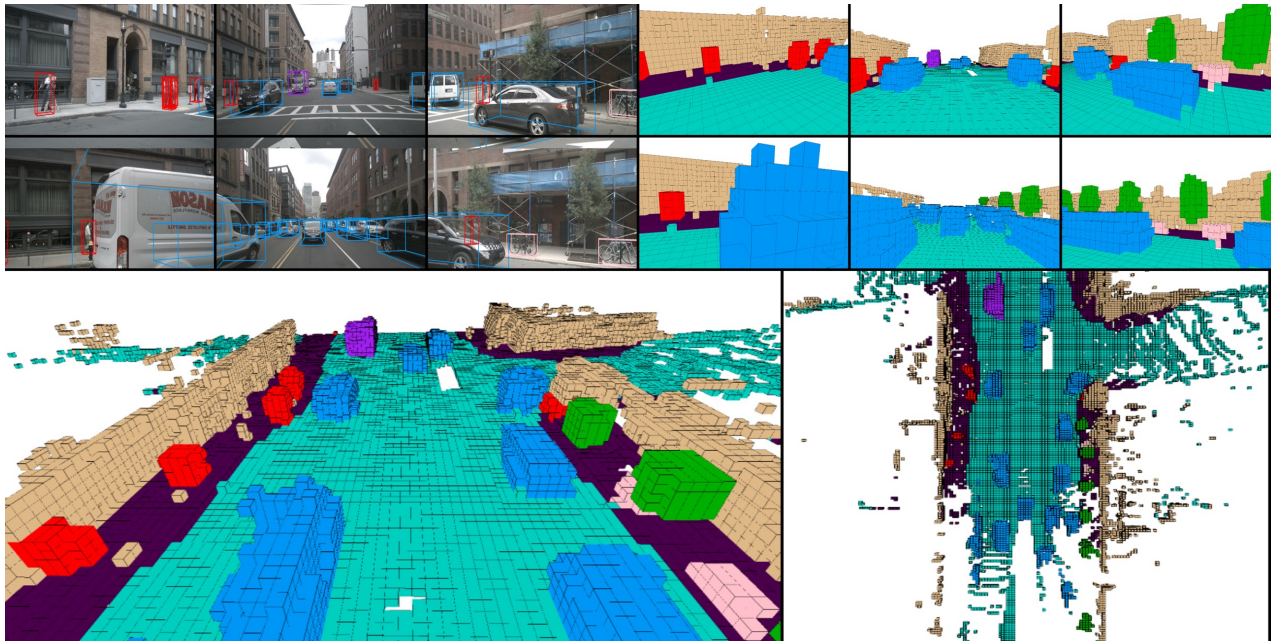


Figure 9. Visualization of 3D occupancy prediction in a narrow urban street with parked and moving vehicles, pedestrians, and bicycles. The top-left shows object detection in the image space, the top-right presents occupancy prediction in the camera view, the bottom-left illustrates the top-front view, and the bottom-right depicts the top-down occupancy prediction results.

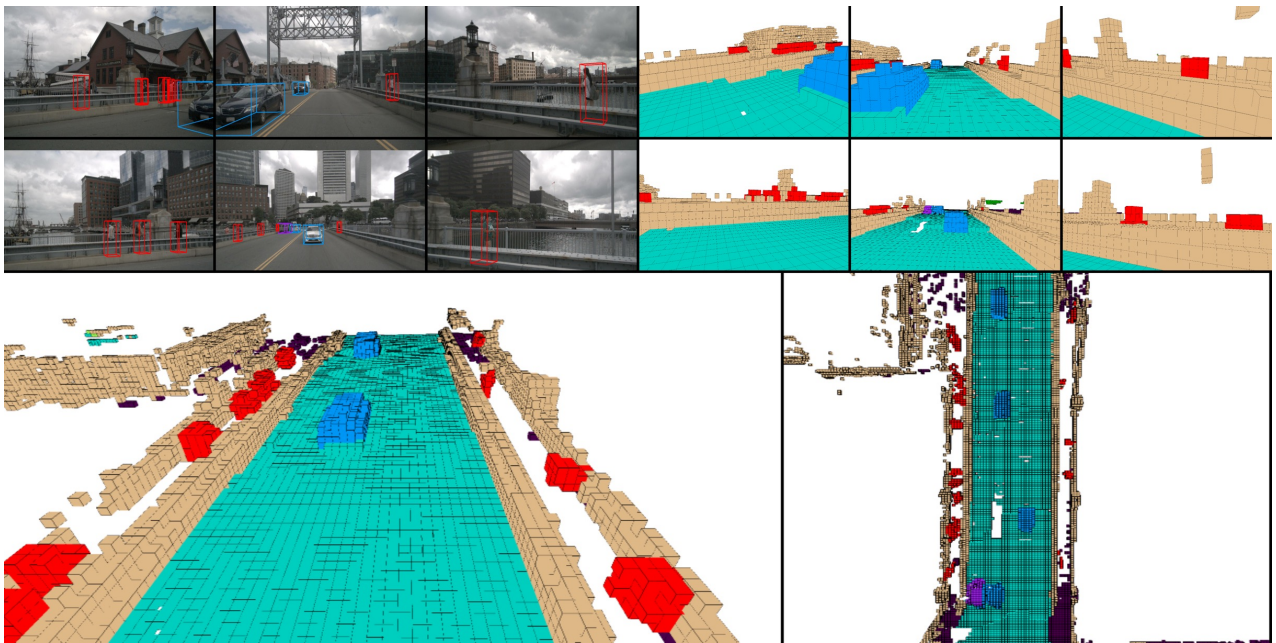


Figure 10. Visualization of 3D occupancy prediction on a bridge with moving vehicles and pedestrians. The top-left shows object detection in the image space, the top-right presents occupancy prediction in the camera view, the bottom-left illustrates the top-front view, and the bottom-right depicts the top-down occupancy prediction results.

- | | | | | | | | | |
|---|--|--|--|---|---|---|--|--|
| ■ barrier | ■ bicycle | ■ bus | ■ car | ■ cons. veh. | ■ motorcycle | ■ pedestrian | ■ traffic cone | ■ trailer |
| ■ truck | ■ drive. surf. | ■ other flat | ■ sidewalk | ■ terrain | ■ manmade | ■ vegetation | ■ others | |